High resolution FTIR study of the ν5, ν6, and ν9 fundamental bands of CH2D37Cl

High resolution FTIR study of the ν_5, ν_6, and ν_9 fundamental bands of $CH_2D^{37}Cl$

Paolo Stoppa [a], Andrea Pietropolli Charmet [a], Alessandra De Lorenzi [a], Filippo Tamassia [b], Mattia Melosso [c], Elisabetta Cané [b], Luca Dore [c], Cristina Puzzarini [c]

Journal of Quantitative Spectroscopy and Radiative Transfer
Volume 270, August 2021, 107719

High resolution FTIR study of the ν_5, ν_6, and ν_9 fundamental bands of $CH_2D^{37}Cl$

Paolo Stoppa [a,*], Andrea Pietropolli Charmet [a], Alessandra De Lorenzi [a], Filippo Tamassia [b], Mattia Melosso [c], Elisabetta Cané [b], Luca Dore [c], Cristina Puzzarini [c]

[a] *Dipartimento di Scienze Molecolari e Nanosistemi, Università Ca' Foscari Venezia, Via Torino 155, 30172 Mestre (VE), Italy.*

[b] *Dipartimento di Chimica Industriale "Toso Montanari", Università di Bologna, Viale Risorgimento 4, 40136 Bologna, Italy.*

[c] *Dipartimento di Chimica "Giacomo Ciamician", Università di Bologna, Via Selmi 2, 40126 Bologna, Italy*

The first high-resolution infrared spectra of $CH_2D^{37}Cl$ have been investigated in the region 650 – 1100 cm^{-1} where the lowest fundamental bands ν_5 (826.2626 cm^{-1}), ν_6 (708.4307 cm^{-1}), and ν_9 (986.3405 cm^{-1}) occur. These vibrations perturb each other by different weak interactions and the $v_5 = 1$ and $v_6 = 1$ states were treated according to a model which accounts for a *c*-type Coriolis resonance. The spectral analysis resulted in the identification of 1664, 2550 and 2657 ro-vibrational transitions for ν_5, ν_6, and ν_9 bands respectively, and to the determination of accurate spectroscopic parameters by using the Watson's *A*-reduction Hamiltonian in the I^r representation. The simulations of the ro-vibrational structure of the ν_5, ν_6, and ν_9 bands performed in different spectral regions adequately reproduce the experimental data.

Keywords: Monodeuterated chloromethane; Infrared spectrum; Spectroscopic parameters; Ro-vibrational analysis.

* Corresponding author:
Tel.: +39 041 234 8513. e-mail address: stoppa@unive.it

1. Introduction

Among the different chlorine-bearing organic molecules present in the Earth's atmosphere, chloromethane (CH_3Cl) is one of the most abundant (around 553 – 559 pptv according to the 2016 data [1]). Natural sources of chloromethane are manifold, comprising not only the oceans but also plants [2], soils [3, 4] and wildfires [5]. The anthropogenic emissions of CH_3Cl are mainly related to chemical activities [6], and coal and biomass burning [5], but recently it has been found also in the human breath [7]. Following the first spectroscopic detection of chloromethane in the atmosphere through the strong ν_1 feature around 3.4 μm [8], its global distribution (in both the upper troposphere and lower stratosphere) has been successfully measured by the ACE-FTS experiment [9, 10].

Being so closely related to biological and anthropogenic activities, it is not surprising that CH_3Cl has been proposed among the most promising biomarkers for the search of potentially habitable exoplanets [11]. Conversely, until a few years ago it was thought that interstellar chlorinated compounds were basically limited only to a few hydrides [12], thus excluding the presence of even simpler organohalides like chloromethane. The recent discovery of chloromethane (with both $CH_3{}^{35}Cl$ and $CH_3{}^{37}Cl$ isotopologues unambiguously detected) in the protostar IRAS 16293-2422 [13] revealed that also this class of compounds must be properly considered and investigated in astrochemistry. Interestingly, many deuterated molecules have been discovered in the same protostar (including also the bi-deuterated isomers) like HDO and D_2O [14], NHD and ND_2 [15, 16] or CH_2DCN and CHD_2CN [17]. These findings suggest that also CH_3Cl might present a relevant deuterium fractionation in IRAS 16293-2422, thus leading to potentially detectable amounts of the monodeuterated form (CH_2DCl) provided that accurate spectroscopic predictions are available. When compared to the large amount of data available for the parent species CH_3Cl, until quite recently only a few investigations were carried out on CH_2DCl thus seriously hampering its spectroscopic detections as well as the accurate determination of the ratio $CH_2D^{35}Cl/CH_2D^{37}Cl$ [18]. Therefore, we decided to support the search of mono-deuterated chloromethane in the interstellar medium by providing accurate spectroscopic data for both the $CH_2D^{35}Cl$ and $CH_2D^{37}Cl$ isotopologues. In our previous work [19] we measured the spectrum of these species in the millimeter region obtaining precise rest frequencies and an accurate set of ground state constants. The present study deals with the infrared spectrum of this molecule; to complement the data already available for $CH_2D^{35}Cl$ [20 – 22] here we report on the ro-vibrational analysis of $CH_2D^{37}Cl$ focusing on the intense absorptions falling in the region between 15.4 and 9.3 μm. This region is characterized by the very strong features of the ν_6 band associated to the C-Cl stretching centered at about 708 cm^{-1}, and by the presence of two fundamentals related to the in-plane C-D bending (ν_5, 826 cm^{-1}) and the C-D/CH_2 out-of-plane

bending (ν_9, 986 cm^{-1}). An accurate set of spectroscopic parameters, also including the modelling of *c*-type Coriolis resonance between the $v_5 = 1$ and $v_6 = 1$ states, have been obtained for all the excited vibrational states presently investigated. These results, together with the previously available ones for the other isotopologue [20 – 22] provide a solid and reliable description of the spectroscopic properties of monodeuterated chloromethane in the infrared portion of the spectrum to support its possible observation and quantification.

2. Experimental details

The $CH_2D^{37}Cl$ sample was prepared by reacting monodeuterated methanol (CDN Isotopes, 99.2% D-enriched) with $Na^{37}Cl$ (Cambridge Isotope Laboratory; 95%-^{37}Cl enriched) in a solution of diluted sulphuric acid, following the method previously described for the ^{35}Cl isotopologue [20]. Evidence of $CH_2D^{35}Cl$ impurities were observed and identified in the infrared spectra of the sample.

The infrared spectra of $CH_2D^{37}Cl$ were recorded at the University of Bologna (Italy) using a Bomem DA3.002 FTIR spectrometer [23, 24] equipped with a globar source, a KBr beamsplitter and a photoconductive mercury cadmium telluride (MCT) detector. The high-resolution (0.004 cm^{-1} unapodized) spectra were recorded at room temperature with sample pressure of 31 Pa and 53 Pa and an optical pathlength of 6 m, achieved with a multipass absorption cell. Eight hundred scans were co-added to improve the signal-to-noise ratio of the spectra. The wavenumber absolute calibration was obtained using ro-vibrational transitions of H_2O and CO_2 from the HITRAN database [25]. The line positions were measured using the OriginPro 2018 software package and the accuracy of measurements for unblended lines was estimated to be ca. 0.001 cm^{-1}. In the investigated range, the measured full width at half maximum (FWHM) is about 0.003 cm^{-1}.

3. General remarks

The CH_2DCl molecule is a nearly-prolate asymmetric-top rotor ($\kappa = -0.978$) belonging to the symmetry point group C_s; the molecular symmetry plane contains the *a*- and *b*- axes, while the *c*-axis is perpendicular to it. Six of the nine vibrational modes are classified of symmetry species A' ($\nu_1 - \nu_6$) and give rise *a*-/*b*-hybrid bands, while three ($\nu_7 - \nu_9$) are of A'' symmetry and produce *c*-type absorptions. The *a*-type component presents a contour similar to that of parallel bands, while the *b*- and *c*-type envelopes are expected to follow that of perpendicular bands of symmetric tops.

In the present investigation were considered the usual selection rules for the *a*- ($\Delta J = 0, \pm1$; $\Delta K_a = 0, \pm2$; $\Delta K_c = \pm1$), *b*- ($\Delta J = 0, \pm1$; $\Delta K_a = \pm1$; $\Delta K_c = \pm1$) and *c*- ($\Delta J = 0, \pm1$; $\Delta K_a = \pm1$; $\Delta K_c = 0, \pm2$) type bands and we have denoted with *even* ($K_a'' + K_c'' = J''$) and *odd* ($K_a'' + K_c'' = J'' + 1$) the levels split by asymmetry.

The rotational energy levels in the ground and excited vibrational states were calculated based on Watson's *A*-reduced Hamiltonian up to the sixth order of the total rotational operator in the I^r representation [26] and adequately implemented with perturbation operators when the interactions were considered. The assigned transitions were treated using the ATIRS package software [27] that contains the Visual CALPGM program, a graphical interface to the SPFIT/SPCAT programs written by Pickett [28].

In the fitting procedure an uncertainty of 0.001 cm^{-1} was attributed to unblended lines while for large or very weak features the uncertainty was set to 0.004 cm^{-1}; badly overlapped features were excluded from the fit.

4. Description of the spectra

A low resolution (0.5 cm^{-1}) survey spectrum of $CH_2D^{37}Cl$ in the region analyzed is illustrated in Fig. 1, where the fundamentals ν_5 (~826 cm^{-1}), ν_6 (~708 cm^{-1}) and ν_9 (~986 cm^{-1}) are indicated.

The ν_6 band is the lowest in wavenumber and the strongest fundamental of $CH_2D^{37}Cl$ and is ascribed to C-Cl stretching; the overview of the investigated region, illustrated in Fig. 1, shows that the *a*-type component is predominant. In the high-resolution spectra the ${}^qP_K(J)$ manifolds present a rotational structure rather compressed and partially unresolved for low *J* values, while in the *R*-branch the individual ${}^qR_K(J)$ clusters cover larger spectral sections and the lines with different K_a values can be identified more easily. A typical example is shown in Fig. 2, where the positions of the K_a features in the ${}^qR_K(32)$ group are marked. The effect of the asymmetry splitting is evident for $K_a = 1, 2, 3$ with

the *even* component lying on the higher wavenumber side; the opposite trend occurs for the ${}^{q}P_K(J)$ manifolds. The *Q*-branch is formed by a series of ${}^{q}Q_K$ groups degrading towards lower wavenumbers for increasing *J*; within each cluster, characterized by a first line with $J = K_a$, the sequence of the lines with the same *J* and $K_a = J - 1, J - 2, \ldots$ values proceeds towards higher wavenumbers. A section of the *Q* branch in the range 707.6 – 708.6 cm^{-1} is depicted in Fig. 3.

The ν_5 vibration is associated with the C-D in-plane bending and gives rise to an *a*-/*b*-hybrid band where the *a*-type component is predominant. The rotational structure of the ${}^{q}P_K(J)$ and ${}^{q}R_K(J)$ clusters in ν_5 is similar to that in ν_6 but spread in a larger spectral range. Conversely, the *Q*-branch, illustrated in Fig. 4, presents a somewhat different structure. The apparent irregular structure of the *Q*-branch of the ν_5 fundamental is due to the strong overlapping of the ${}^{q}Q_K(J)$ manifolds; the strongest line of each multiplet corresponds to $J = K_a$ and the K_a-lines progression decreases both in wavenumber and intensity.

The ν_9 vibration mainly corresponds to the C-D/CH_2 out-of-plane bending and the fundamental is a typical *c*-type band with strong ${}^{p,r}Q_K(J)$ clusters fully resolved. In absence of asymmetry doubling, observed up to $K_a'' = 3$, each ${}^{p}Q_K(J)$ and ${}^{r}Q_K(J)$ cluster degrades to lower wavenumber as *J* increases, thus indicating that $(B + C)/2$ of $v_9 = 1$ is smaller than that of the ground state one. Two typical multiplets are illustrated in Fig. 5, where the different degradation due to the asymmetry splitting is clearly visible.

The structure of the ${}^{p}P_K(J)$ and ${}^{r}R_K(J)$ subbranches is clear and spread out all over the spectral region investigated (895 – 1077 cm^{-1}); the weak ${}^{r}P_K(J)$ and ${}^{p}R_K(J)$ transitions were also identified and included in the dataset.

5. Results and discussion

The analysis of ν_6 of $CH_2D^{37}Cl$ started with the identification of the resolved details of the ${}^{q}P_K(J)$ and ${}^{q}R_K(J)$ clusters using predicted values and considering the ro-vibrational structure of the same band of $CH_2D^{35}Cl$ [20]. The preliminary calculations were performed by setting the band origin at 708.43 cm^{-1} [20] and employing the very recent ground state constants [19] for both ground and upper state. Then, new predictions with higher *J* and K_a quantum numbers were made, providing further assignments and new refinements, and so forth.

As this iterative procedure progressed, we noticed a deterioration of the fit's standard deviation and a significant difference in the value of the Δ_{JK} parameter between the ground and $v_6 = 1$ state.

Although we did not notice any irregularities in the resolved structure of the band, this led us to suppose that the $v_6 = 1$ state interacts with the $v_5 = 1$ level as found for the ^{35}Cl isotopologue [20]. These vibrational states belong to the same symmetry species, hence may interact by *c*-type Coriolis perturbation ($\Delta K_a = \pm1, \pm3, \ldots$ and $E^{\pm} \leftrightarrow O^{\mp}$) and/or anharmonic resonance ($\Delta K_a = 0, \pm2, \ldots$ and $E^{\pm} \leftrightarrow E^{\pm}$ or $O^{\pm} \leftrightarrow O^{\pm}$) where the + and – signs refer to *even* ($K_a + K_c = J$) and *odd* ($K_a + K_c = J + 1$) levels, respectively. We tried to consider both types of interaction but only the former led to satisfactory results by employing a *c*-type Coriolis operator in the form:

$$\widehat{H}^c = i(\xi^c_{5,6}\,\hat{P}_c + \xi^{c,J}_{5,6}\hat{P}_c\hat{P}^2) \qquad (1)$$

where $\hat{P}$ and $\hat{P}_c$ are the operators of the angular momentum and its component along the *c* principal inertial axis, respectively.

Employing the set of constants obtained from the analysis of the *a*-type component, we tried to identify the *b*-type transitions but they turned out to be too weak to be reliably recognized and therefore no rotational analysis was performed for this component.

Line identification in the ν_5 band was carried out following a similar procedure. In comparison to those of the ν_6, the ${}^qP_K(J)$ and ${}^qR_K(J)$ manifolds of ν_5 are more resolved and the assignment was proved simple enough. On the contrary the *Q*-branch is very compressed (see Fig. 4) and only some strong ${}^qQ_K(J)$ lines could be reliably assigned. As in the ν_6 band, no transitions of the *b*-type component could be assigned in the ν_5 band with confidence.

The results obtained from the simultaneous fit of 4214 transitions of the ν_5 and ν_6 bands are collected in Table 1 which also includes, besides the ground and $v_9 = 1$ state constants (see later), the maximum value of J' and K_a' of the fitted transitions. As shown, the standard deviation of 5.61 x 10^{-4} cm^{-1} is well within the experimental accuracy of the measurements. The difference between the upper and ground state values does not exceed 0.7% for the rotational constants and 5.7% for the centrifugal distortion terms except for the δ_J of the $v_5 = 1$ state which differs by 17.4%. The value of the Φ_{KJ} distortion term of the upper states was constrained to that of the ground state; since the value of this constant is very small a satisfactory determination would have been obtained using transitions with higher K_a values than those fitted in the present work. Also, the δ_K distortion term of $v_5 = 1$ was fixed to that of the ground state because when it was refined an unreliable value was obtained having an error of 46% and differing by 51% from the ground state value. The large deviation with respect to the ground state for the δ_J and δ_K of the $v_5 = 1$ state indicates that some contribution of resonances was not accordingly accounted for by the model. Therefore, we considered

possible interactions between $v_5 = 1$ and $v_9 = 1$. In this case, being the vibrations of symmetry A' and A", respectively, the states may interact through *a*-type (with selection rules ΔK_a = 0, ±2, … and $E^{\pm} \leftrightarrow E^{\mp}$ or $O^{\pm} \leftrightarrow O^{\mp}$) as well as *b*-type ($\Delta K_a$ = ±1, ±3, … and $E^{\pm} \leftrightarrow O^{\pm}$) Coriolis resonances. However, the use of the corresponding perturbation operators for the calculation of the rotational term values did not lead to a significant improvement of the fit.

The starting point of the ν_9 band analysis was the assignment of the ${}^{p}Q_K(J)$ and ${}^{r}Q_K(J)$ clusters considering the predicted values and the structure of $CH_2D^{35}Cl$ ν_9 fundamental [21]. The assigned transitions were used to obtain a set of more accurate upper state constants which was employed for the identification of new lines. The refinement procedure was iteratively applied until the assignment was completed in the entire spectral range investigated. No strong spectral irregularities were observed in the ro-vibrational structure of the band and the data were fitted according to a model for an unperturbed rovibrational state. The best set of the spectroscopic parameters determined for the $v_9 = 1$ is reported in Table 1. The standard deviation (6.56 x 10^{-4} cm^{-1}) is smaller than the estimated accuracy of the measurements and none of the deviations between observed and calculated line positions was found in absolute value higher than 0.002 cm^{-1}. The obtained constants for this vibrational state compare reasonably well with those of the ground state with the exception of δ_J, which differs by 20%. Since this difference was considerably greater for δ_K its value was fixed to that of the ground state; this was not unexpected since transitions with K_a values much higher are needed to get a reliable value for this constant. The outliers of the δ_J and δ_K distortion parameters confirm the presence of weak interactions with the $v_5 = 1$ state. It is interesting to note that (see Table 1) the differences of the δ_J value of the $v_5 = 1$ and $v_9 = 1$ states with respect to the ground one are similar in magnitude but opposite in sign. In order to evaluate how the different resonances can affect the ro-vibrational levels, a K_a energy diagram for the $v_5 = 1$, $v_6 = 1$, and $v_9 = 1$ vibrational states was calculated using the parameters of Table 1. The diagram confirms the *c*-Coriolis resonance between the $v_5 = 1$ and $v_6 = 1$ states and shows that the $v_5 = 1$ level can be perturbed by the $v_6 = 1$ and $v_9 = 1$ levels through high-order interactions. However, since no irregularities in the resolved structure of the bands analyzed in the present work as well as in the residuals (i.e., observed – calculated values) have been found, these interactions must be rather weak.

To test the quality of the parameters obtained in the present work, spectral simulations in different spectral regions of the ν_5, ν_6, and ν_9 fundamentals were performed. The synthetic spectra were obtained using the constants of Table 1 and adopting a Lorentzian line profile with a linewidth (FWHM) of 0.003 cm^{-1} at the temperature of 298 K. As can be seen in the Figs. 2 – 5, the calculated

features (upper trace) match well with the observed ones thus confirming the reliability of the constants obtained.

A complete list of all fitted transitions is deposited as supplementary material.

6. Conclusions

A detailed ro-vibrational study of the lowest fundamentals ν_5, ν_6, and ν_9 of $CH_2D^{37}Cl$ occuring in the region $650 - 1100$ cm^{-1} has been performed for the first time. The analysis of the high-resolution infrared spectra led to identify of a large number of ro-vibrational transitions of the bands and to the determination of accurate spectroscopic parameters. The adequacy of the experimental data reproduction is confirmed by the good match between simulated and experimental spectra in the overall investigated region. The constants of the $v_5 = 1$ and $v_6 = 1$ states were obtained according to a model which accounted for a *c*-type Coriolis resonance whereas the $v_9 = 1$ state has been considered unperturbed. However, the large difference of the δ_J value in $v_5 = 1$ and $v_9 = 1$ with respect to that in the ground state suggests the existence of a weak *a*- or *b*- type Coriolis resonance between these levels.

The spectroscopic parameters obtained in the present work can be useful for supporting and guiding the detection of the different isotopologues of CH_3Cl in astronomical spectra.

Acknowledgements

This work has been supported by University Ca' Foscari Venezia (ADiR funds) and by Bologna University (RFO funds). The authors gratefully remember Mr. A. Baldan for the preparation of the $CH_2D^{37}Cl$ sample.

Appendix A. Supporting information

Supplementary data associated with this article (a complete list of fitted transitions) can be found in the online version at ...

References

[1] Engel A, Rigby M, Burkholder JB, Fernandez RP, Froidevaux L, Hall BD, Hossaini R, Saito T, Vollmer MK, Yao B. Update on ozone-depleting substances (ODS) and other gases of interest to the Montreal Protocol, Scientific Assessment of Ozone Depletion: 2018, World Meteorological Organization, Geneva, Switzerland, 2018, ch.1.

[2] Umezawa T, Baker AK, Brenninkmeijer CAM, Zahn A, Oram DE, van Velthoven PFJ. Methyl chloride as a tracer of tropical tropospheric air in the lowermost stratosphere inferred from IAGOS-CARIBIC passenger aircraft measurements. J Geophys Res Atmos 2015; 120; 313 – 326.

[3] Shechner M, Guenther A, Rhew R, Wishkerman A, Li Q, Blake D, Lerner G, Tas E. Emission of volatile halogenated organic compounds over the various Dead Sea landscapes. Atmos Chem Phys 2019; 19; 7667 – 7690.

[4] Keppler F, Röhling AN, Jaeger N, Schroll M, Hartmann SC, Greule M. Sources and sinks of chloromethane in a salt marsh ecosystem: constraints from concentration and stable isotope measurements of laboratory incubation experiments. Environ Sci Proc & Impacts 2020; 22; 627 – 641.

[5] Andreae MO, Merlet P. Emission of trace gases and aerosols from biomass burning. Global Biogeochem Cycles 2001; 15; 955 – 966.

[6] Li S, Park M-K, Jo CO, Park S. Emission estimates of methyl chloride from industrial sources in China based on high frequency atmospheric observations. J Atmos Chem 2017; 74; 227 – 243.

[7] Keppler F, Fischer J, Sattler T, Polag D, Jaeger N, Schöler HF, Greule M. Chloromethane emissions in human breath. Sci Total Environ 2017; 605 – 606; 405 – 410.

[8] Park JH, Zander R, Farmer CB, Rinsland CP, Russell JM, Horton RH, et al. Geophys Res Lett 1986; 13; 765 – 768.

[9] Kaley AW, Weigum N, McElcheran C, Taylor JR. Global methyl chloride measurements from the ACE-FTS instrument. International Symposium on Molecular Spectroscopy Department of Chemistry the Ohio State University, TI-09; 2009.

[10] Brown AT, Volk CM, Schoeberl MR, Boone CD, Bernath PF. Stratospheric lifetimes of CFC-12, CCl_4, CH_4, CH_3Cl and N_2O from measurements made by the Atmospheric Chemistry Experiment-Fourier Transform Spectrometer (ACE-FTS). Atmos Chem Phys 2013; 13; 6921 – 6950.

[11] Schwieterman EW, Kiang NY, Parenteau MN, Harman CE, DasSarma S, Fisher TM, Arney GN, Hartnett HE, Reinhard CT, Olson SL, Meadows VS, Cockell CS, Walker SI, Grenfell JL, Hegde S, Rugheimer S, Hu R, Lyons TW. Exoplanet Biosignatures: A Review of Remotely Detectable Signs of Life. Astrobiology 2018; 18; 663 – 708.

[12] Neufeld DA, Wolfire MG. The chemistry of interstellar molecules containing the halogen elements. ApJ 2009; 706; 1594.

[13] Fayolle EC, Öberg KI, Jørgensen JK, Altwegg K, Calcutt H, Müller HSP, Rubin M, van der Wiel MHD, Bjerkeli P, Bourke TL et al. Protostellar and cometary detections of organohalogens. Nat Astron 2017; 1; 703 – 708.

[14] Coutens A, Vastel C, Caux E, Ceccarelli C, Bottinelli S, Wiesenfeld L,et al. A study of deuterated water in thelow-mass protostar IRAS 16293-2422. Astron Astrophys 2012; 539; A132.

[15] Melosso M, Bizzocchi L, Sipilä O, Giuliano BM, Dore L, Tamassia F, Martin-Drumel M-A, Pirali O, Redaelli E, Caselli P. First detection of NHD and ND_2 in the interstellar medium: Amidogen deuteration in IRAS 16293-2422. Astron Astrophys 2020; 641; A153.

[16] Bacmann A, Faure A, Hily-Blant P, Kobayashi K, Ozeki H, Yamamoto S, Pagani L, Lique F. Deuterium fractionation of nitrogen hydrides: Detections of NHD and ND_2. MNRAS 2020; 499; 1795 – 1804.

[17] Calcutt H, Jørgensen J, Müller H, Kristensen L, Coutens A, Bourke T., et al. The ALMA-PILS survey: complex nitriles towards IRAS 16293-2422. Astron Astrophys 2018; 616; A90.

[18] Wallström SHJ, Muller S, Roueff E, Le Gal R, Black JH, Gérin M. Chlorine-bearing molecules in molecular absorbers at intermediate redshifts. A&A 2019; 629; A128.

[19] Melosso M, Achilli A, Tamassia F, Canè E, Pietropolli Charmet A, Stoppa P, Dore L. High-resolution millimeter-wave spectroscopy of CH_2DCl: Paving the way for future astronomical observations of chloromethane isotopologues. J Quant Spectrosc Ra 2020; 248; 106982.

[20] Baldacci A, Stoppa P, Pietropolli Charmet, Giorgianni S, Nivellini G, High resolution FTIR study of the ν_5 and ν_6 bands of $CH_2D^{35}Cl$: analysis of resonances and determination of ground and upper state constants. Mol Phys 2005; 103: 2803 – 811.

[21] Baldacci A, Visinoni R, Giorgianni S, Nivellini G, High-resolution FTIR spectroscopy of $CH_2D^{35}Cl$: rovibrational analysis of the ν_3, ν_9 fundamentals and the $2\nu_6 - \nu_6$, $\nu_5 + \nu_6 - \nu_6$ hot bands. Mol Phys 2008; 106: 1233 – 1240.

[22] Baldacci A, Visinoni, Nivellini G, High-resolution FTIR spectroscopy of $CH_2D^{35}Cl$: analysis of the nearly degenerate ν_4 and ν_8 levels. Mol Phys 2010; 108: 2395 – 2410.

[23] Bizzocchi L, Tamassia F, Laas J, Giuliano BM, Degli Esposti C, Dore L, Melosso M, et al. Rotational and high-resolution infrared spectrum of HC_3N: global ro-vibrational analysis and improved line catalog for astrophysical observations. Astrophys J Suppl Ser 2017; 233: 11.

[24] Tamassia F, Melosso M, Dore L, Pettini M, Canè E, Stoppa P, Pietropolli Charmet A. Spectroscopy of a low global warming power refrigerant. Infrared and millimeter-wave spectra of trifluoroethene (HFO-1123) in the ground and some vibrational excited states. J Quant Spectrosc Ra 2020; 248: 106980.

[25] Gordon IE, Rothman LS, Hill C, Kochanov RV, Tan Y, Bernath PF, Birk M, et al. The HITRAN2016 molecular spectroscopic database. J Quant Spectrosc Ra 2017; 203: 3–69.

[26] Watson JKG. Vibrational spectra and structure, Vol. 6. New York/Amsterdam: Elsevier (Ed. J. R. Durig); 1977.

[27] Tasinato N, Pietropolli Charmet A, Stoppa P. ATIRS package: A program suite for the rovibrational analysis of infrared spectra of asymmetric top molecules. J Mol Spectrosc 2007; 243: 148–154.

[28] Pickett HM. The fitting and prediction of vibration-rotation spectra with spin interactions. J Mol Spectrosc 1991; 148: 371–377.

Figure Captions

Figure 1. Section of the low-resolution (0.5 cm^{-1}) spectrum of $CH_2D^{37}Cl$; room temperature, optical path length = 6 m, P = 130 Pa.

Figure 2. Rotational structure of the ${}^{q}R_K(32)$ cluster of the ν_6 band of $CH_2D^{37}Cl$. Upper trace: simulated spectrum. Lower trace: experimental spectrum (P = 31 Pa) showing the details of the ${}^{q}R_K(32)$ cluster; *even* and *odd* refer to ($K_a'' + K_c'' = J''$) and ($K_a'' + K_c'' = J'' + 1$) transitions, respectively. Lines marked by asterisks belong to the ν_6 band of $CH_2D^{35}Cl$.

Figure 3. Spectral portion of the *Q*-branch of the ν_6 band of $CH_2D^{37}Cl$. Some lines belonging to the ${}^{q}Q_K(8)$, ${}^{q}Q_K(10)$ and ${}^{q}Q_K(12)$ manifolds are indicated. Upper trace: simulated spectrum. Lower trace: experimental spectrum (P = 31 Pa).

Figure 4. Spectral portion of the *Q*-branch of the ν_5 band of $CH_2D^{37}Cl$ where the structure of the ${}^{q}Q_K(8)$, ${}^{q}Q_K(9)$ and ${}^{q}Q_K(10)$ manifolds is indicated. Upper trace: simulated spectrum. Lower trace: experimental spectrum (P = 31 Pa).

Figure 5. Portion of the *even* and *odd* ${}^{p}Q_2(J)$ manifolds of the ν_9 band of $CH_2D^{37}Cl$ showing the large effect of asymmetry doubling. Upper trace: simulated spectrum. Lower trace: experimental spectrum (P = 53 Pa); *even* and *odd* refer to ($K_a'' + K_c'' = J''$) and ($K_a'' + K_c'' = J'' + 1$) transitions, respectively.

Figure 1

Click here to access/download;Figure;Figure1.tif

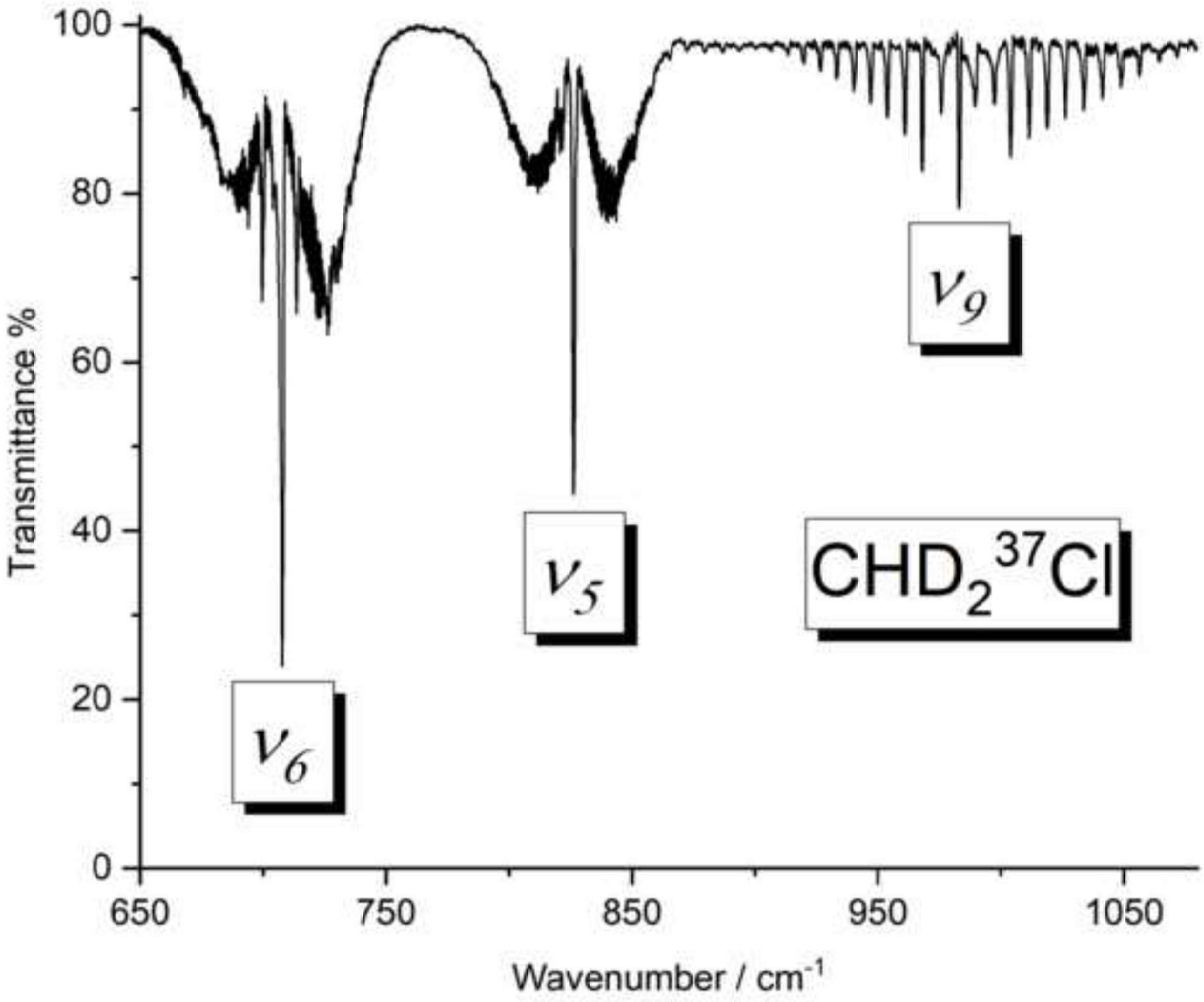

Figure 2

Click here to access/download;Figure;Figure2.tif

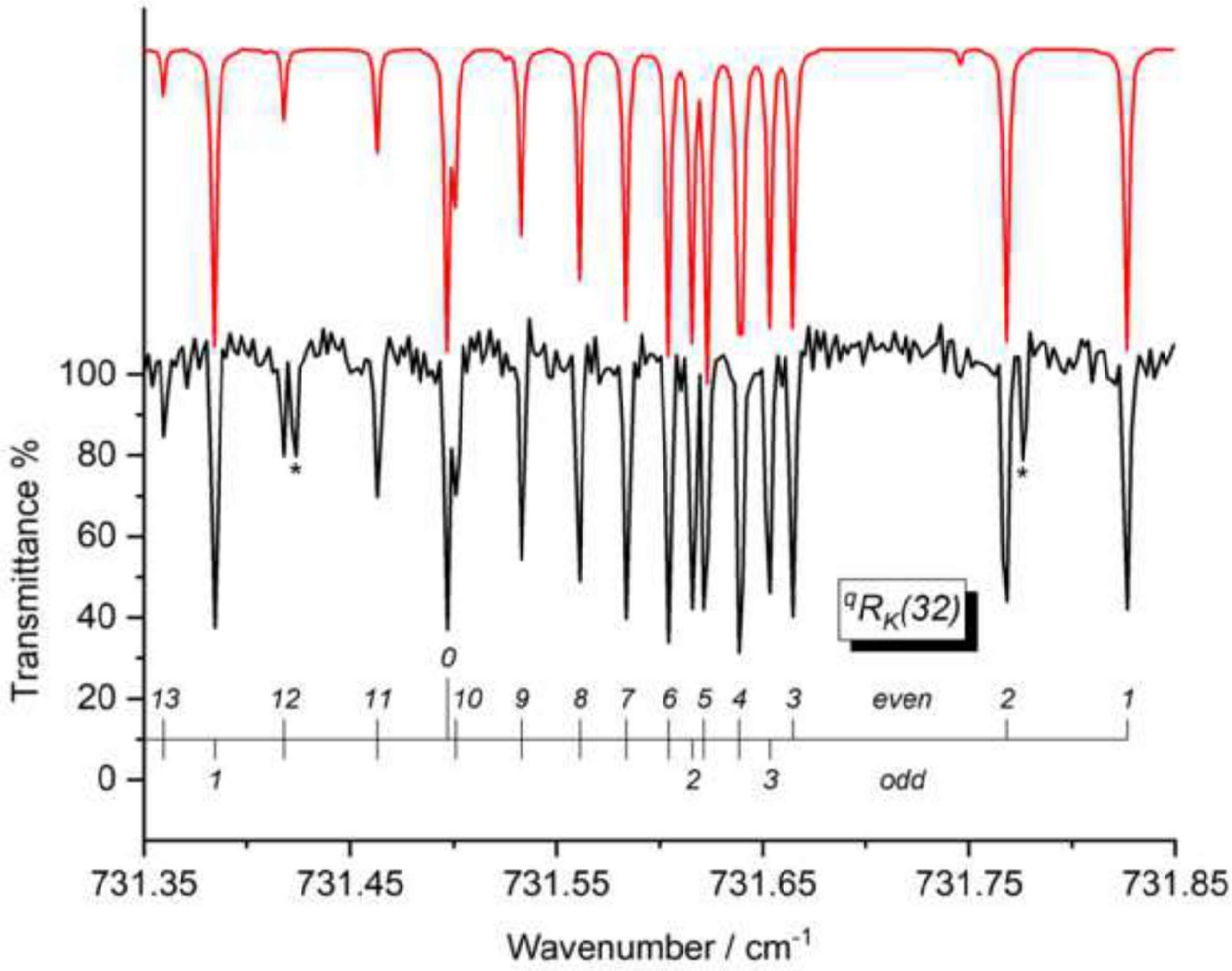

Figure 3

Click here to access/download;Figure;Figure3.tif

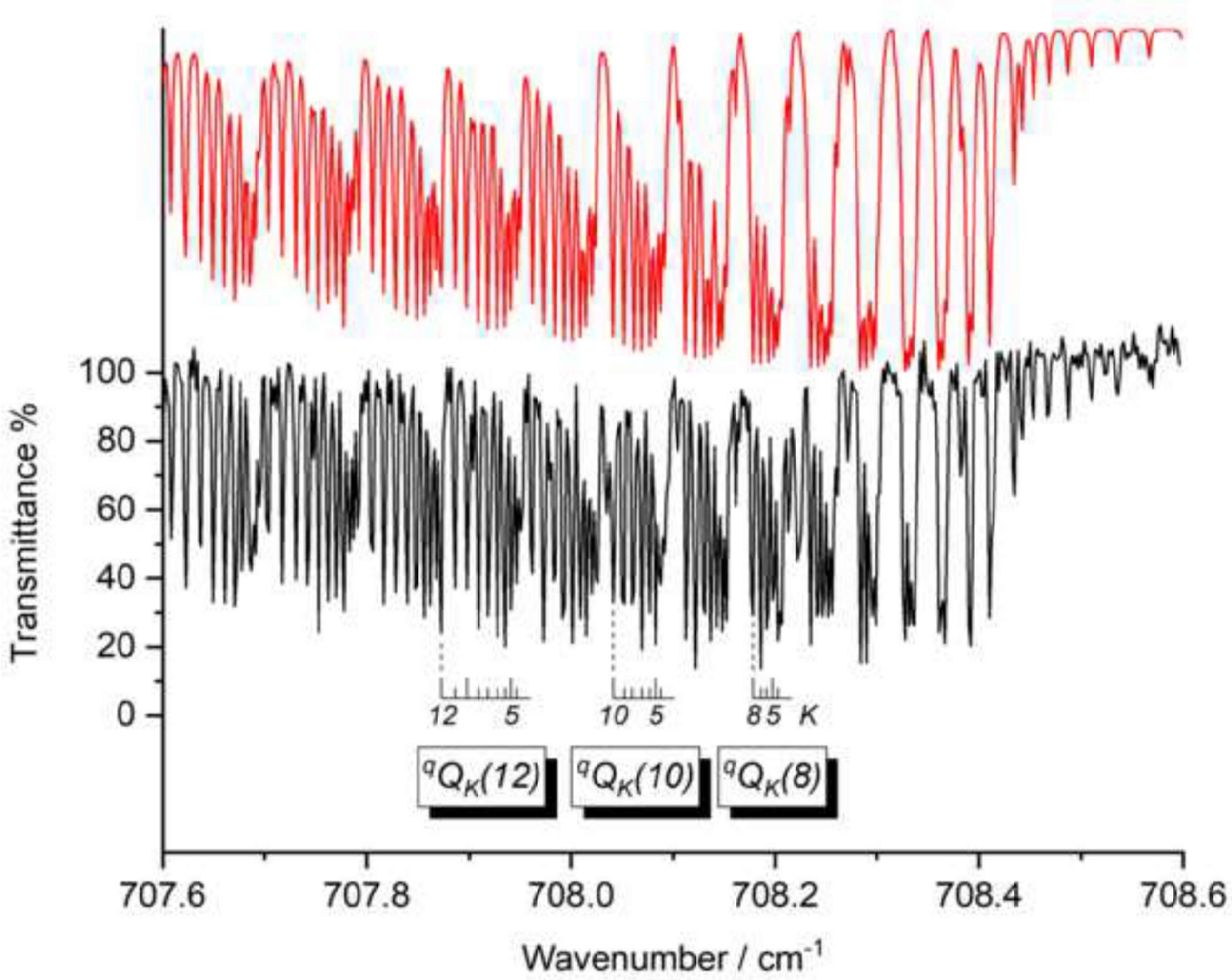

Figure 4

Click here to access/download;Figure;Figure4.tif

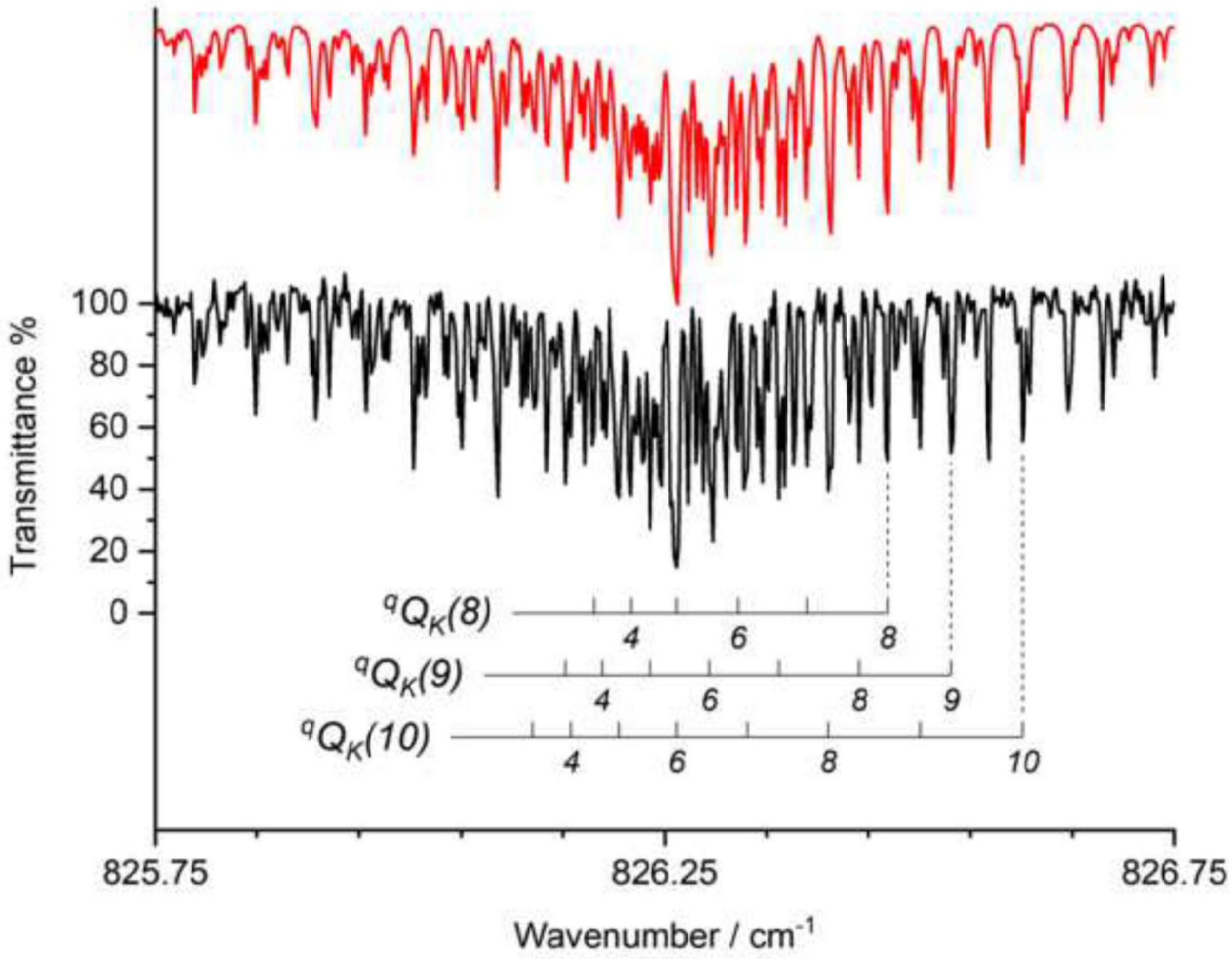

Figure 5

Click here to access/download;Figure;Figure5.tif

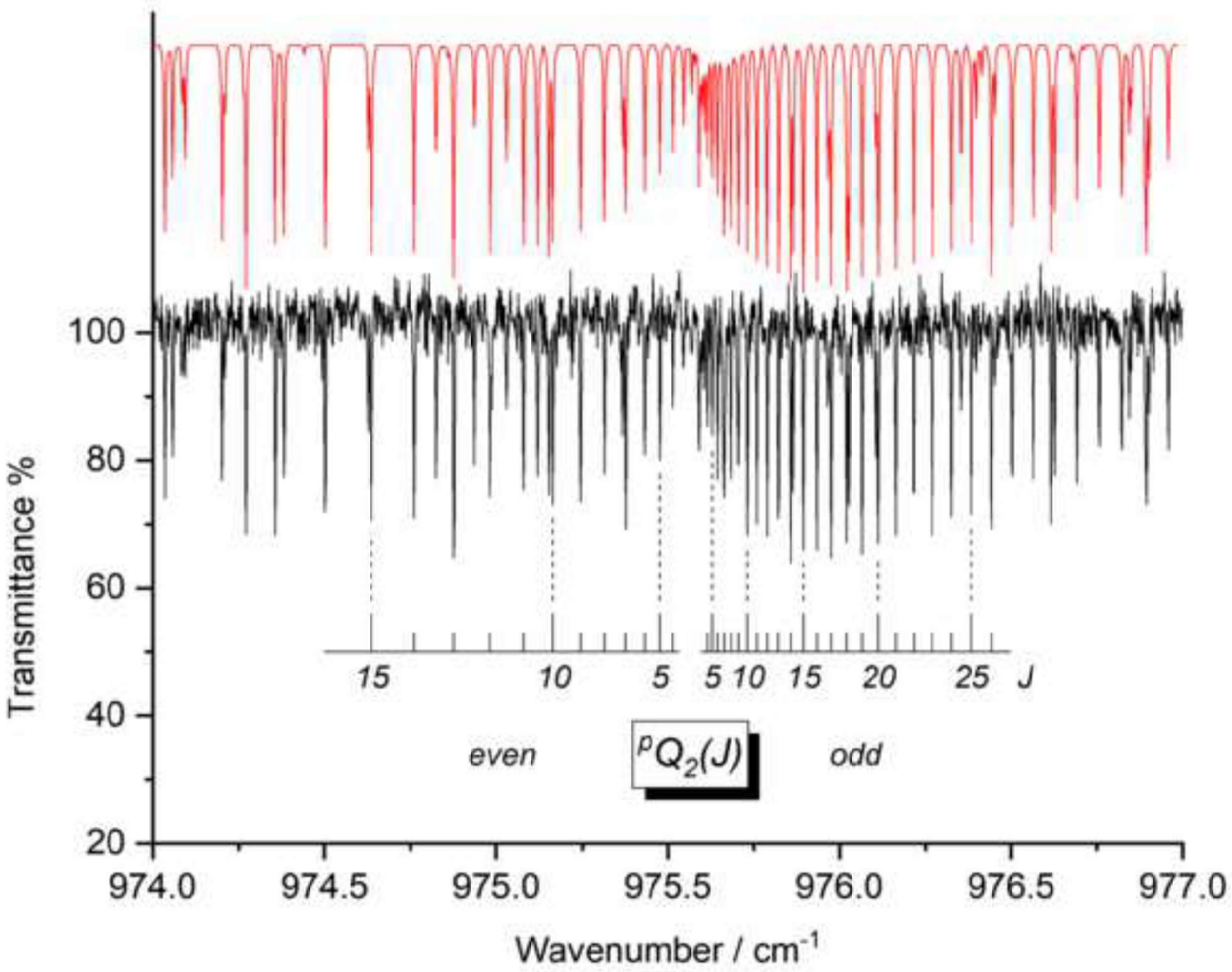

Table 1. Spectroscopic parameters (cm^{-1}) of the $v_5 = 1$, $v_6 = 1$ and $v_9 = 1$ states of $CH_2D^{37}Cl$ [a]

	Ground State [b]	$v_5 = 1$	$v_6 = 1$	$v_9 = 1$
ν_0		826. 262445(84)	708.430689(94)	986.340520(68)
A	3.9972629	4. 0008953(32)	3.9937307(28)	4.0232222(39)
B	0.40955340	0.40785304(54)	0.40663171(46)	0.40847734(53)
C	0.39979232	0.39817122(117)	0.39683473(110)	0.39836778(52)
Δ_J x 10^6	0.48624	0.47727(34)	0.49589(33)	0.487207(137)
Δ_{JK} x 10^5	0.50687	0.49512(37)	0.51850(35)	0.55568(36)
Δ_K x 10^4	0.5523	0.545147(173)	0.555571(140)	0.59343(45)
δ_J x 10^7	0.1153	0.0953(20)	0.121884(163)	0.138729(197)
δ_K x 10^6	0.682	0.682 [c]	0.698(96)	0.682 [c]
Φ_{KJ} x 10^9	0.121	0.121 [c]	0.121 [c]	0.121 [c]
$\xi^c_{5,6}$			0.15714(39)	
$\xi^{c,J}_{5,6}$ x 10^5			–0.170(23)	
No. data fitted		1664	2550	2657
J'_{max}, $K_a'_{max}$		49, 15	54, 15	43, 10
σ x 10^3 (cm^{-1})			0.561	0.656

[a] Quoted uncertainties are one standard deviation in units of the last significant digit. Except Φ_{KJ}, the value of all the sextic centrifugal distortion constants were fixed to zero.
[b] From Ref. [19].
[c] Fixed to the ground state value.